ASSESSMENT OF SIX DIFFERENT METHODS FOR THE ESTIMATION OF SURFACE ULTRA-VIOLET FLUXES AT ONE LOCATION IN URUGUAY

Claire Thomas[1], Agustín Laguarda Cirigliano[2], William Wandji Nyamsi[3], Antti Arola[3], Uwe Pfeifroth[4], Jörg Trentmann[4], Thierry Ranchin[5], and Lucien Wald[5]

[1] Transvalor S.A., Biot (France)

[2] Laboratorio de Energía Solar, Universidad de la República, Montevideo (Uruguay)

[3] Finnish Meteorological Institute, Kuopio (Finland)

[4] Deutscher Wetterdienst, Satellite Application Facility on Climate Monitoring, Offenbach (Germany)

[5] MINES ParisTech, PSL University, O.I.E. Laboratory, Sophia Antipolis (France)

Abstract

This communication assesses six methods estimating Ultra-Violet A and B (UV-A and UV-B) fluxes from satellite imagery, numerical weather models or ground measurements. The UV estimates from each method are compared to coincident 15 minutes in-situ measurements collected at one location in Uruguay from September 2015 to January 2019. The first method combines Global Horizontal Irradiance (G) measured on site with satellite-derived daily Ozone concentration. The second method uses an empirical model onto satellite-retrieved solar broadband irradiance at the surface (SSI) produced by HelioClim-3 version 5 (HC3v5) to derive UV fluxes. The third method named CAMS-UV, is one of the outputs of ECMWF numerical weather model. The three remaining methods rely on more sophisticated modelling of the atmosphere in cloud-free conditions using radiative transfer modelling combined to a cloud modification factor (or cloud extinction) derived from HC3v5. Outside an underestimation observed for the UV-B range for both CAMS-UV (-20 %) and for the empirical model (-29 %), methods demonstrated their ability to collect the temporal variability of the signal of the instrument on-ground; biases ranges from -2 to 4 % for UV-A and from 0 to 10 % for UV-B, RMSE are close to 15 % and almost all correlation coefficients exceed 0.96. This analysis gives precious elements for discussion about the performance of models mainly developed and validated over Europe and Africa.

Keywords: UV-A and B, CAMS, HelioClim-3, surface solar irradiance, radiative transfer modeling, numerical weather model, ground measurements

1. Introduction

Solar Ultra-Violet (UV) radiation at ground level has beneficial but also negative effects on human health and ecosystems. UV-B radiation, which ranges in [280, 315] nm, is the most energetic part of the solar spectrum that reaches the ground; and is responsible for instance for the damage of DNA leading in rare cases to skin cancers and melanomas (Coste et al., 2015; Fortes et al., 2016, Savoye et al., 2016). Interest is growing in the role of UV-A [315, 400] nm and UV [280, 400] nm in their benefit for diverse brain diseases such as migraines (Lisicki et al., 2017), Parkinson's disease (Kravietz et al., 2017), and other diseases such as thyroid cancer (Mesrine et al., 2017) or sclerosis (Orton et al., 2011). UV plays a significant role in water disinfection as one of the three common water treatment technologies (Kosjek et al., 2009).

Researchers would ideally like to handle long-term, homogeneously distributed and available worldwide UV datasets. Unfortunately, due to high cost of UV radiometers and maintenance, these measurements are scarce. Alternatives have consequently been developed to derive UV radiation from broadband Global Horizontal Irradiance (G) or from numerical weather models. This communication presents the validation results of 6 different methods to assess UV-A and UV-B at 1 site in Uruguay. It represents a unique opportunity to investigate how models originally developed and validated over Europe and Africa perform for this site in South America.

2. Ground measurements

Ground measurements are the property of the laboratory of solar energy, from the University of the Republic, Montevideo in Uruguay. The geographical coordinates of the site are -31.2821° for the latitude, -57.9176° for the longitude, and finally 50 m for the altitude. It is located in the North West quarter of Uruguay, near the border of Argentina. Figure 1 depicts the location of the Uruguayan site in the world map of Köppen-Geiger climate classification (Peel et al., 2007). This classification proposes to divide climates into five main climate groups, with each group being divided based on seasonal precipitation and temperature patterns. The site is located in the center of a "Cfa" code zone (green), corresponding to a humid subtropical climate.
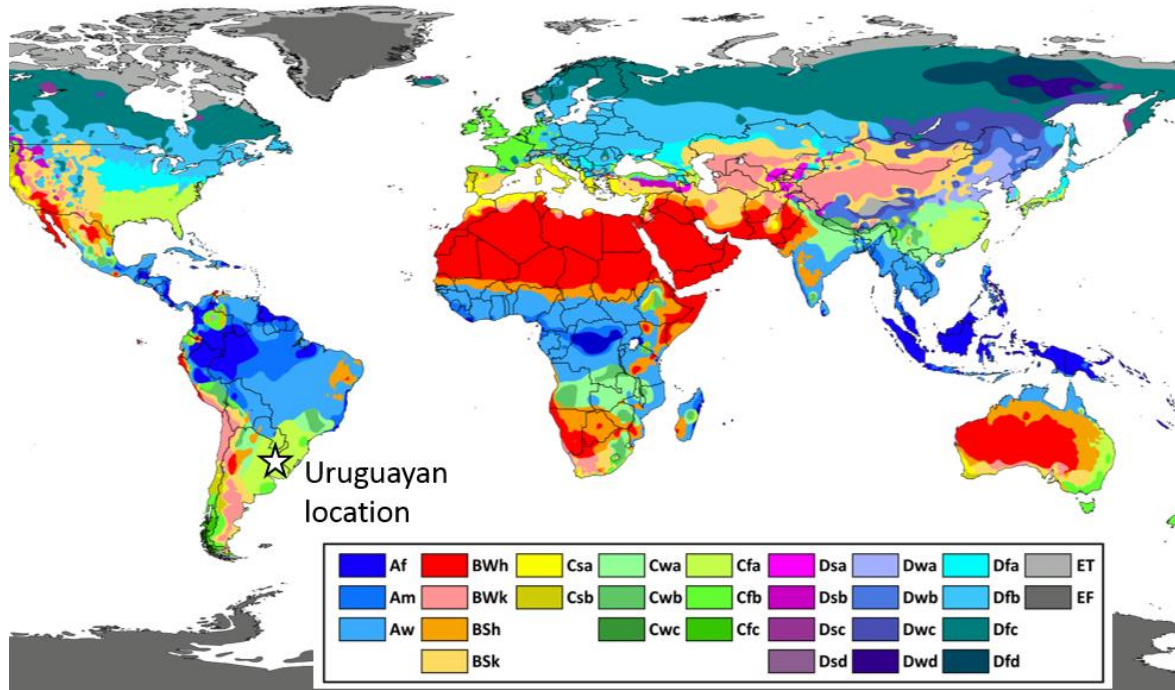

Fig. 1: Location of the Uruguayan site in the world map of Köppen-Geiger climate classification. The location corresponds a humid subtropical climate (code "Cfa", Peel et al., 2007)

In-situ measurements corresponds to 15 minute UV-A and UV-B measurements collected with Kipp and Zonen UV radiometers with controlled temperature. UV-B data are available from June 2017 to Jan. 2019, and UV-A from Oct. 2015 to Jan. 2019, with a gap from Nov. 2016 to June 2017. Data are irradiances in W m^{-2} in local time (universal time minus 3 hours). 15 min irradiances were generated by averaging 1 minute samples only if more than 66 % of the 1 minute samples were available, corresponding to a minimum of 10 slots for the synthesis of the 15 minute dataset. 1 minute irradiances are the results from the averaging of 6 instantaneous measurements collected every 10 seconds, once again only if 100 % of the 10 second samples were available (no holes).

UV-A and UV-B measurements are considered only when the solar elevation angle is above 7°, and when G measured at the same location exceeds 15 W m^{-2}. As the site is equipped with high quality instruments and the station is very well maintained, the visual inspection didn't emphasize the need an additional quality check algorithm.

3. Description of the six methods estimating UV irradiances

3.1. Method #1: Locally-adapted AM

"AM" stands for Antón Martínez, author of the method and described in his PhD thesis (2007). The parametrization of this empirical model applies onto in-situ G and satellite-derived (OMI/TOMS) daily ozone concentration. We expect that this method outperforms other methods.

3.2. Method #2: Wald

Global set of coefficients has been empirically designed to derive UV-A and UV-B from broadband G produced by the surface solar irradiance (SSI) HelioClim-3 version 5 (HC3v5) using the model Heliosat-2 (Blanc et al., 2011, Rigollier et al., 2004). This method has been applied in the past for instance to generate monthly average maps of

UV daily doses within the EUROSUN project (Wald 2012), and in the analysis of the influence of UV radiation in the occurrences and intensity of migraines (Lisicki et al., 2017).

3.3. Method #3: CAMS-UV FMI

The CAMS-UV processor is part of a global model running on ECMWF servers. It produces global UV index (UVI) and spectral UV forecasts on demand to users. The CAMS-UV spatial resolution is approximately 80 km before 21st June 2016 at 12 UTC and approximately 40 km later on. It does not depend on the geographical point. These data are provided with a temporal sampling rate of 1 hour for UVI and 3 hours for UV-A and UV-B. For the sake of this analysis, the temporal sampling rate has been artificially decrease to 15 minutes by using a temporal linear interpolation of the 1-hourly UVI cloud modification factor i.e. ratio between all-sky UVI and clear-sky UVI, and 15 min clear-sky UV estimates derived from Modified Lambert-Beer approach (Mueller et al., 2004) applied on two closest 3-hourly UV estimates. Of course, this means that the 3-hourly estimates are more reliable than high temporal resolution estimates. A complete description of the CAMS-UV processor and quarterly validation reports are regularly updated on the CAMS website (active in Aug. 2019): https://atmosphere.copernicus.eu/

3.4. Method #4a: Weighted_Kato HC3v5 and Method #4b: Discretized_Kato HC3v5

These methods rely on the assumption that broadband G can be accurately retrieved from a reduced number of spectral bands (Kato et al., 1999, Lefèvre et al., 2013). CAMS McClear uses several look up tables (LUT) computed by the Radiative Transfer Model libRadtran for selected values of inputs and provides the irradiance in cloud-free conditions for each of the 32 spectral intervals. The Weighted_Kato method (Wandji Nyamsi et al., 2017) corresponds to weights applied on the 6 first Kato bands to supply UV-A and UV-B datasets. The Discretized_Kato method proposes a spectral resampling to refine the results based on a few additional parameters and interpolations. An all-sky version of these methods is obtained by extracting a cloud modification factor (or clear-sky index) from HC3v5, with the underlying assumption that clouds are not spectrally sensitive.

3.5. Method #5: DWD SARAH-3

Very similar in principle to Weighted_Kato method, SPECMAGIC also consists of LUT generated for each of the 32 Kato bands (Mueller et al., 2012). Its cloud-free estimates are combined with spectrally-resolved cloud transmission values derived with radiative transfer corrections of the broadband cloud transmission. Spectral irradiances are scheduled to be available together with the next generation of broadband SSI provided by the Climate Monitoring Satellite Application Facility (CM-SAF) in 2021.

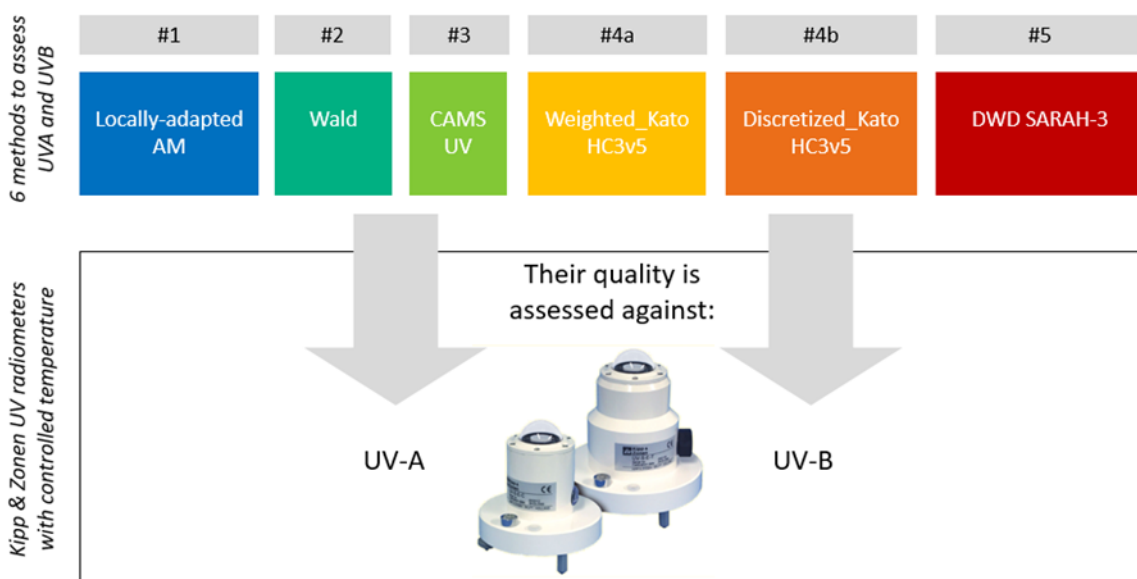Figure 2 provides a recapitulative scheme of the assessment of the performance of these 6 UV-methods.

Fig. 2: Recapitulative scheme of the quality assessment of the 6 methods to derive UV-A and UV-B, against the measurements at a site in Uruguay.

4. Validation protocol and results

The selected protocol is the usual one; time and space coincident estimates are compared to the corresponding measurements. Night values are discarded. Correlation coefficients (CC) are computed. The sets of differences (estimates-minus measurements) are computed and summarized by their bias and the standard deviation (STDEV) as these two indices are fully independent. Relative values are computed by dividing the bias or the STDEV by the mean of the measurements and are given in percent. Results are available in Tab. 1 and 2 for UV-B and UV-A respectively. 2-D histograms between measurements and estimates are displayed in Fig. 3 and 4. Green color highlights best results while orange color highlights worst ones without results of the method #1.

Tab. 1: UV-B in [280, 315] nm, number of coincident measurements: 19936. Mean of the in-situ measurements: 0.9 W m–2. Green color highlights best results while orange color highlights worst ones without results of the method #1

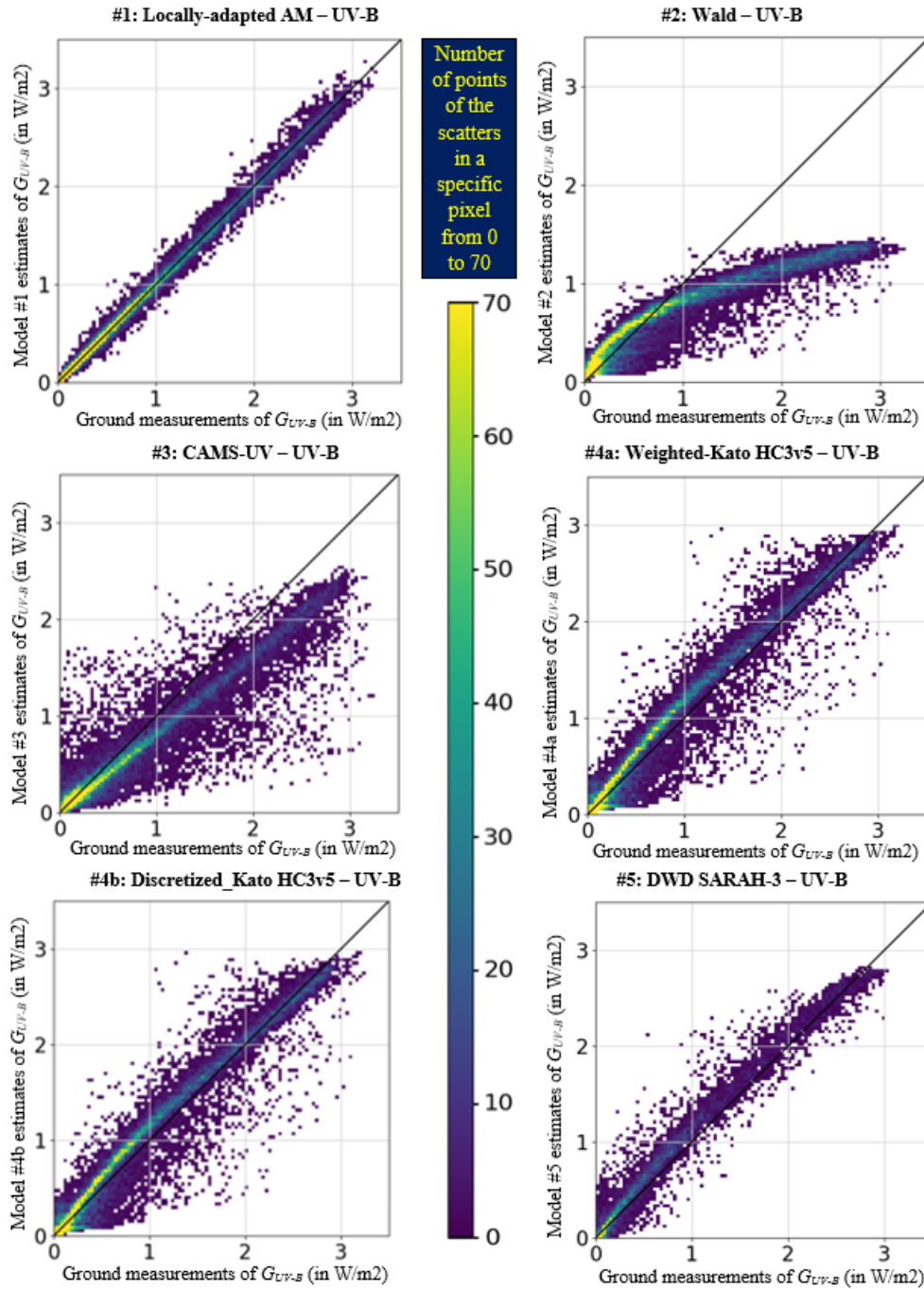|	Method	Bias (W m^{-2}) and relative value	STDEV (W m^{-2}) and relative value	CC
#1	Locally-adapted AM	0 (0 %)	0 (4.4 %)	0.997
#2	Wald	-0.2 (-28.5 %)	0.3 (38.6 %)	0.930
#3	CAMS-UV	-0.2 (-19.3 %)	0.2 (27.2 %)	0.931
#4a	Weighted_Kato HC3v5	0.1 (6.2 %)	0.1 (16.3 %)	0.971
#4b	Discretized_Kato HC3v5	0 (4.1 %)	0.1 (15.1 %)	0.972
#5	DWD SARAH-3	0.1 (10.1 %)	0.1 (15.6 %)	0.978

Fig. 3: 2-D histograms of the UV-B derived from the 6 different models (vertical axes) and UV-B in-situ measurements (horizontal axis). Models are respectively: #1 Locally-adapted AM, #2 Wald, #3 CAMS-UV, #4a Weighted_Kato HC3v5, #4b Discretized_Kato HC3v5, and #5 DWD SARAH-3

Tab. 2: UV-A in [315, 400] nm, number of coincident measurements: 32269. Mean of the in-situ measurements: 24.9 W/m2. Green highlights best results while orange highlights poorest ones outside method #1

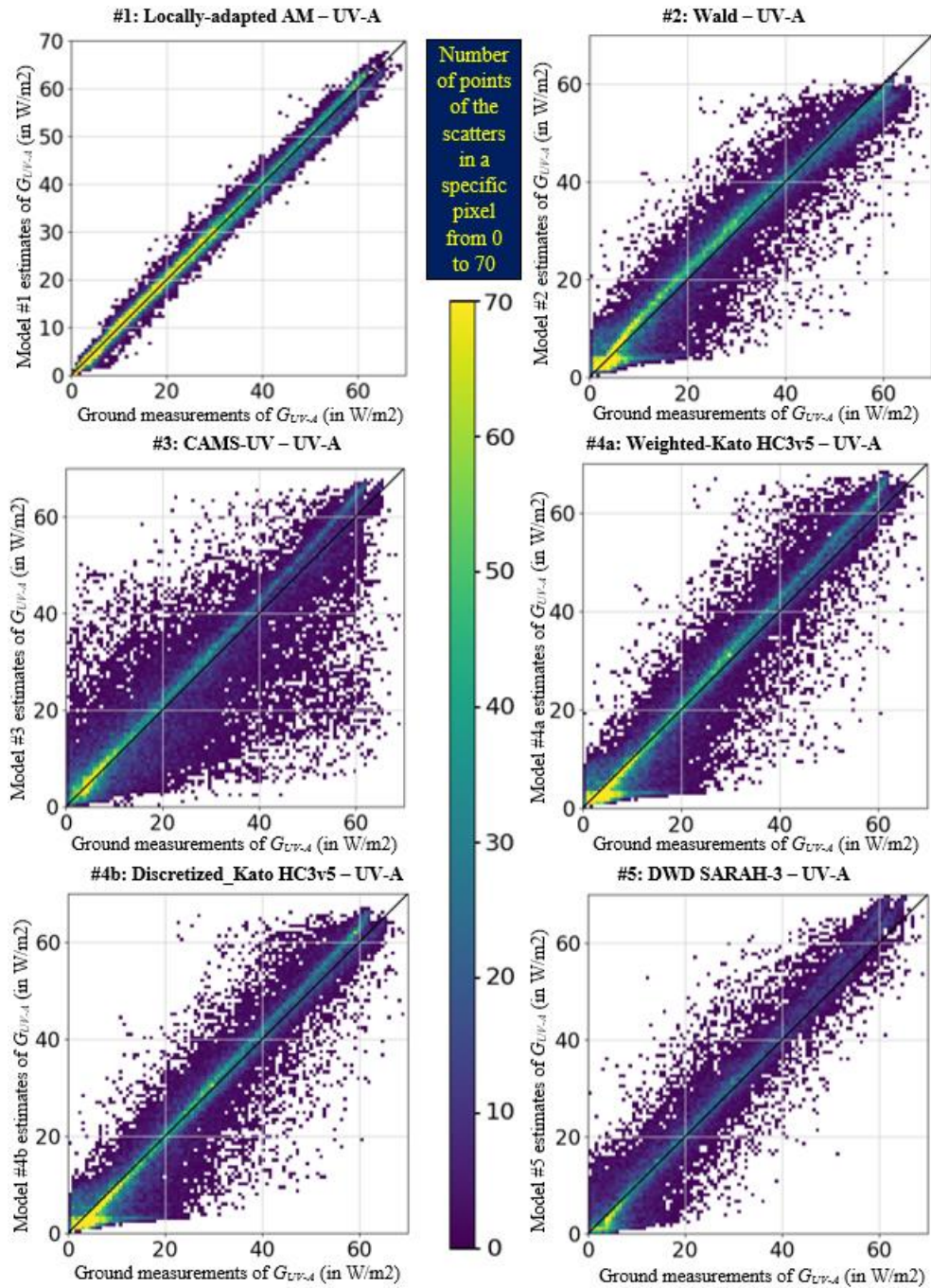|	Method	Bias (W/m2) and relative value	STDEV (W/m2) and relative value	CC
#1	Locally-adapted AM	0 (0 %)	1.06 (4.3 %)	0.997
#2	Wald	0 (0 %)	3.37 (13.6 %)	0.959
#3	CAMS-UV	-0.6 (-2.3 %)	5.87 (23.5 %)	0.856
#4a	Weighted_Kato HC3v5	0.2 (0.6 %)	3.57 (14.4 %)	0.961
#4b	Discretized_Kato HC3v5	-0.4 (-1.6 %)	3.39 (13.6 %)	0.961
#5	DWD SARAH-3	1 (4.2 %)	3.58 (14.4 %)	0.964

Fig. 4: 2-D histograms of the UV-A derived from the 6 different models (vertical axes) and UV-A in-situ measurements (horizontal axis). Models are respectively: #1 Locally-adapted AM, #2 Wald, #3 CAMS-UV, #4a Weighted_Kato HC3v5, #4b Discretized_Kato, and #5 DWD SARAH-3

5. Validation protocol and results

As expected, the method #1 (locally-adapted AM) outperforms others for both UV-B and UV-A spectral ranges. The good fit between the model and the in-situ measurements is characterized by a narrow cloud of points well-aligned along the y=x axis on the 2-D histograms. Statistical indices show a null bias, a STDEV of about 4 % and CC to its ideal value of 1 with 0.997. This method requires a preliminary training of the parameters using in-situ G which offers the possibility to appropriately capture the local temporal variability, leading to an almost excellent fit with the in-situ UV measurements.

Method #2 (Wald) shows an eyebrow shape on the 2-D histogram for the UV-B range. Despite a good correspondence of low irradiances, large UV-B irradiances are strongly underestimated. This discrepancy is confirmed by the lowest performances in all statistical results: Bias is -0.2 W m^{-2} corresponding to a relative bias of -28.5 %, STDEV is 0.3 W/m2 (38.6 %), but with still a good correlation with a value of 0.93.

Wald method depicts surprisingly very good results for the UV-A range, with a null bias and a STDEV of 3.4 W m^{-2} (13.6 %). CC is lower than expected with a value of 0.959. An explanation of this loss of correlation is the presence of a yellow cluster of points for low UV-A irradiances, as if a threshold of 5 W/m2 was applied onto satellite UV-A irradiances. This phenomenon is also observed on UV-A 2-D histograms for both Weighted_Kato HC3v5 and Discretized_Kato HC3v5. The common parameter is the use of the broadband G from HC3v5. One of the potential reasons for such artefact could be the reflection of the light on the Earth's surface in the satellite direction. Also named "sun glint". This phenomenon has a drastic effect on the Heliosat-2 methods (Blanc et al., 2011, Rigollier et al., 2004) used to update HC3 in real time. Indeed, white reflectances in Meteosat images are considered as clouds, leading to erroneously low irradiances at ground level. A further analysis would consist of identifying and discarding instants potentially affected by the sun glint in order to inspect the impact on 2-D histograms.

The 2-D histogram for the method #3 (CAMS-UV) and for the UV-B range shows a line which goes through the point (0, 0), but with an underestimation of the large UV-B irradiances. The angle between the y=x line and the line of the cloud of points is approximately 5°. The underestimation is confirmed by a negative bias of -0.2 W m^{-2} (-19.3 %). The scattering of the cloud of points is quite large with a STDEV of 0.2 W/m2 (27.2 %). CC is close to Wald UV-B one with 0.931. This observation concerning the large scattering of the points is also valid for the UV-A range; despite a good bias of -0.6 W m^{-2} (-2.3 %), STDEV is the largest one compared to all methods with 5.9 W m^{-2} (23.5 %), and CC is the poorest with 0.856. This can be explained by the fact that CAMS-UV is one of the outputs of ECMWF numerical weather model which operates on a coarser grid (80 km before 21st June 2016 at 12 UTC and approximately 40 km later on) than satellite ones with a spatial resolution of approximately 7 km for this location.

Methods #4a (Weighted_Kato HC3v5) and #4b (Discretized_Kato HC3v5) rely on the same method, while method #4b applies a refinement compared to #4a with the objective to reach a better representation of the solar spectrum. In that perspective, results should be similar, with a slight enhancement of #4b. Validation results for UV-B coincide with this observation, with a bias for method #4a of 0.1 W/m2 (6.2 %) and for method #4b 0.03 W/m2 (4.1 %), STDEV values are very close, with a value of approximately 0.1 W/m2 (16 %) and CC of 0.97. For the UV-A range, method #4a obtains a low bias of 0.2 W/m2 (0.6 %), whereas #4b slightly underestimates the in-situ measurements with a bias of -0.4 W/m2 (-1.6 %). STDEV and CC, very similar for both methods, are 3.4 W/m2 (14 %) and 0.961 respectively. Anyway, biases below a few percent means than the models are close to the uncertainty of the ground instrument, and consequently can be considered as excellent, as it was already the case for the Wald method for the UV-A range.

As for the two previous methods, Method #5 (DWD SARAH-3) is also based on the 32 wavelength intervals of the solar spectrum as defined by Kato et al. (1999). Consequently, it is coherent to observe a similar scattering of the points in the 2-D histograms, in agreement with STDEV values respectively of 0.1 W m^{-2} (15.6 %) for UV-B and 3.6 W m^{-2} (14.4 %) for UV-A. This method shows a lower performance in terms of bias with values of 0.1 W m^{-2} (10.1 %) for the UV-B range and 1 W m^{-2} (4.2 %) for UV-A. It is nevertheless very important to notice the increase of performance if one only focuses on CC, with values of 0.978 for the UV-B range and 0.964. The inspection of the 2-D histograms gives essential clues on the interpretation of the results. For UV-A histograms for the three Kato-based methods, one observes that all clusters of points are almost identical and modelled by a line located slightly above the y=x line, as a testimony of a slight overestimation. For #4a and #4b, the overestimation is counterbalanced by the underestimation of low values due to the yellow artefact, as explained in a previous paragraph. This artefacts impacts directly CC, and that is why method #5 outperforms the two other methods referring only to CC.

6. Perspectives

Method #1 (Locally-adapted AM) differs from the other methods as adjusted on local measurements. It would be interesting to evaluate the performance of this method when applied onto satellite SSI retrievals.

Method #2 (Wald) is straightforward, by applying coefficients directly onto the broadband G of a SSI. Consequently, it is computationally economic, and could run easily in real time for the monitoring of a large number of locations. As the Wald method provides excellent results for the UV-A range, one may explore the possibility to correct model parameters to discard the eyebrow shape of the 2-D histogram in the UV-B range.

Method #4b (Discretized_Kato HC3v5) requires a discretization every 1 nm of the Method #4a (Weighted_Kato HC3v5) as a step further for a better adequacy in the results. According to the similarity of the results, this

refinement turns out to be unnecessary. This observation should be confirmed at other locations.

Another perspective of improvement for this work is the investigation of the potential issue of sun glint that could affect HC3v5 for this location, which indirectly impacts methods #2, #4a and #4b mainly for UV-A range.

An extension of this validation work is planned to check if conclusions drawn here could be generalized to other sites and under other climates: Lille (north of France), Observatoire of Haute Provence (south east of France), La Réunion Island (France), and Reading (south of the United Kingdom).

7. Conclusion

This paper proposes a unique opportunity to confront six methods to assess UV for a humid subtropical climate at one site in Uruguay. The method locally-adapted AM provides the best results as expected, since a preliminary training of the parameters is required based on local measurements.

All other methods are either based on satellite imagery or numerical weather model. For the UV-B range, all methods based on the Kato decomposition of the solar spectrum propose very promising results. The output CAMS-UV from ECMWF numerical weather model gives also satisfactory results outside an underestimation that could easily be corrected by a post-bias adjustment. The Wald method would require also a more complex adjustment to correct the underestimation to reach satisfactory results. This work could be worse it as this method is compatible with an operational exploitation in real time.

In the UV-A range and despite a larger scattering of the CAMS-UV histogram, one may conclude that all methods provide a trustful representation of the local temporal variability of the irradiances.

This work is part of a larger project of comparison of methods to assess different methods to supply UV estimates for several sites in the world. The plan is to extend this validation for other sites in France and in the United-Kingdom.

8. References

Blanc, P., Gschwind, B., Lefèvre, M., Wald, L., 2011: The HelioClim project: Surface solar irradiance data for climate applications. Remote Sens., 3, 343-361.

Coste, A., Goujon, S., Boniol, M., Marquant, F., Faure, L., Doré, J.-F., Hémon, D., Clavel, J., 2015. Residential exposure to solar ultraviolet radiation and incidence of childhood hematological malignancies in France, Cancer Cause. Control, 26, 1339–1349.

Fortes, C., Mastroeni, S., Bonamigo, R., Mannooranparampil, T., Marino, C., Michelozzi, P., Passarelli, F., Boniol, M., 2016. Can ultraviolet radiation act as a survival enhancer for cutaneous melanoma? Eur. J. Cancer Prev., 25, 34–40.

Kato, S., Ackerman, T., Mather, J., Clothiaux, E., 1999. The k-distribution method and correlated-k approximation for short-wave radiative transfer model, J. Quant. Spectrosc. Ra., 62, 109–121.

Kosjek, T., Andersen, H.R., Kompare, B., Ledin, A., Heath, E., 2009. Fate of carbamazepine during water treatment, Environ. Sci. Technol., 43 (16), 6256-6261.

Kravietz, A., Ka, S., Wald, L., Dugravot, A., Singh-Manoux, A., Moisan, F., Elbaz, A., 2017. Association of UV radiation with Parkinson disease incidence: a nationwide French ecologic study, Env. Res., 154, 50-56.

Lefèvre, M., Oumbe, A., Blanc, P., Espinar, B., Gschwind, B., Qu, Z., Wald, L., Schroedter-Homscheidt, M., Hoyer-Klick, C., Arola, A., Benedetti, A., Kaiser, J. W., Morcrette, J.-J., 2013. McClear: a new model estimating downwelling solar radiation at ground level in clear-sky conditions, Atmos. Meas. Tech., 6, 2403–2418.

Lisicki, M., D'Ostilio, K., Erpicum, M., Schoenen, J., Magis, D., 2017. Sunlight irradiance and habituation of visual evoked potentials in migraine: The environment makes its mark. Cephal., 38 (7), 1351-1360.

Martínez, M.A., 2007. Modelos empíricos para la estimación de la irradiancia solar ultravioleta. Doctoral dissertation from la Universidad de Extremadura, facultad de ciencias, Departamento de Física.

Mesrine, S., Kvaskoff, M., Bah, T., Wald, L., Clavel–Chapelon, F., Boutron-Ruault, M.-C., 2017. Nevi ambient ultraviolet radiation and thyroid cancer risk: a French prospective study. Epidem., 28 (5), 694–702.

Mueller, R., Dagestad, K. F., Ineichen, P., Schroedter, M., Cros, S., Dumortier, D., Kuhlemann, R., Olseth, J. A., Piernavieja, G., Reise, C., Wald, L., and Heinnemann, D., 2004. Rethinking satellite based solar irradiance modelling –The SOLIS clear sky module, Remote Sens. Environ., 91(2),160–174.

Mueller, R., Behrendt, T., Hammer, A., Kemper, A., 2012. A New Algorithm for the Satellite-Based Retrieval of Solar Surface Irradiance in Spectral Bands. Remote Sens. 4, 622-647.

Orton, S.-M., Wald, L., Confavreux, C. B., Vukusic, S., Krohn, J. P., Ramagopalan, S.V., Herrera, B.M., Sadovnick, A.D., Ebers, G.C., 2011. Association of UV radiation with multiple sclerosis prevalence and sex ratio in France, Neurology, 76 (5), 425-431.

Peel, M. C., Finlayson, B. L., McMahon, T. A., 2007. Updated world map of the Köppen-Geiger climate classification. Hydrol. Earth Syst. Sci., 11, 1633-1644.

Rigollier, C., Lefèvre, M., Wald, L., 2004. The method Heliosat-2 for deriving shortwave solar radiation from satellite images. Sol. Energy, 77, 159-169.

Savoye, I., Olsen, C., Whiteman, D., Bijon, A., Wald, L., Dartois, L., Clavel-Chapelon, F., Boutron-Ruault, M. C., Kvaskoff, M., 2018. Patterns of ultraviolet radiation exposure and skin cancer risk: the E3N-SunExp study, Journal of Epidem., 2018, 28(1), 27-33.

Wald, L., 2012. Elements on the computation of UV maps in the Eurosun database. Internal Report, 2012.

Wandji, W. N., Pitkänen, M. R. A., Aoun, Y., Blanc, P., Heikkilä, A., Lakkala, K., Bernhard, G., Koskela, T., Lindfors, A. V., Arola, A., 2017. A new method for estimating UV fluxes at ground level in cloud-free conditions, Atmos. Meas. Techn., Eur. Geosc. Union, 10 (12), 4965-4978.